Monthly Notices
of the
ROYAL ASTRONOMICAL SOCIETY

MNRAS **456,** 109–118 (2016) doi:10.1093/mnras/stv2640

Combined constraints on deviations of dark energy from an ideal fluid from *Euclid* and *Planck*

Elisabetta Majerotto,[1⋆] Domenico Sapone[2⋆] and Björn Malte Schäfer[3⋆]

[1] *Instituto de Física Teórica, Universidad Autónoma Madrid, C/ Nicols Cabrera 13-15, Cantoblanco, E-28049 Madrid, Spain*
[2] *Cosmology and Theoretical Astrophysics group, Departamento de Física, FCFM, Universidad de Chile, Blanco Encalada 2008, Santiago, Chile*
[3] *Astronomisches Recheninstitut, Zentrum für Astronomie der Universität Heidelberg, Philosophenweg 12, D-69120 Heidelberg, Germany*

Accepted 2015 November 7. Received 2015 October 26; in original form 2015 June 23

ABSTRACT

Cosmological fluids are commonly assumed to be distributed in a spatially homogeneous way, while their internal properties are described by a perfect fluid. As such, they influence the Hubble expansion through their respective densities and equation-of-state parameters. The subject of this paper is an investigation of the fluid-mechanical properties of a dark energy fluid, which is characterized by its sound speed and its viscosity apart from its equation of state. In particular, we compute the predicted spectra for the integrated Sachs–Wolfe effect for our generalized fluid, and compare them with the corresponding predictions for weak gravitational lensing and galaxy clustering, which had been computed in previous work. We perform statistical forecasts and show that the integrated Sachs–Wolfe signal obtained by cross-correlating *Euclid* galaxies with *Planck* temperatures, when joined to galaxy clustering and weak lensing observations, yields a percent sensitivity on the dark energy sound speed and viscosity. We prove that the iSW effect provides strong degeneracy breaking for low sound speeds and large differences between the sound speed and viscosity parameters.

Key words: gravitational lensing: weak – methods: analytical – cosmic background radiation – cosmology: theory – large-scale structure of Universe.

1 INTRODUCTION

The expansion dynamics of the Universe is usually described by assuming (i) general relativity as the theory of gravity, (ii) a high degree of symmetry, namely spatial isotropy and homogeneity at each instant in time, and (iii) ideal fluids which source the gravitational fields. These three assumptions lead to the Friedmann equations for the time-evolution of the scalefactor $a(t)$, which reflect the fact that Einstein's field equations are of second order, and show acceleration or deceleration ä as phenomena.

The inclusion of the cosmological constant on grounds of Lovelock's theorem, which states that the GR field equations are the most general ones in four dimensions, that derivatives of the metric need to be included up to second order, that the energy–moment tensor is conserved, yields a natural way to explain cosmic acceleration at late times.

Alternatively, one can introduce dynamical dark energy components based on scalar self-interacting fields, and interpret the energy–momentum tensor with the corresponding conservation law. This allows the identification of the homogeneous and isotropic field with a relativistic ideal fluid, whose relation between pressure and density is parametrized by an equation of state $w = p/\rho$. At the same time, this equation of state is the only free function that is allowed by Einstein's field equations with the symmetry assumptions of the Robertson–Walker metric.

For these reasons, a central goal of cosmology is to investigate dark energy and the cosmological constant through their influence on the dynamics of the scalefactor and on the growth of structures. The fluid picture is attractive due to its generality. Apart from actual substances like relativistic components ($w = +1/3$) and non-relativistic components ($w = 0$), it is general enough to describe spatial curvature ($w = -1/3$) and the cosmological constant ($w = -1$). Moreover, the isotropy and homogeneity of the fluid ensure the Friedmann symmetries.

Dark energy models based on self-interacting scalar fields show a natural variation of the dark energy equation-of-state parameter. This is because their time evolution is governed by the Klein–Gordon equation, and therefore the kinetic and potential terms in their energy–momentum tensor evolve, leading to a time evolution in the equation of state. Therefore, their influence on the expansion dynamics of the Universe will vary in time. In the slow-roll limit one recovers values of w close to -1, resulting in accelerated expansion.

Adopting a fluid picture is an important test of whether the dark energy fluid is ideal or not. If the fluid has inhomogeneities: (i) pressure fluctuations and density fluctuations are related through a sound speed c_s^2, (which in the most straightforward case describes

⋆E-mail: elisabetta.majerotto@uam.es (EM); dsapone@ing.uchile.cl (DS); bjoern.malte.schaefer@uni-heidelberg.de (BMS)

an adiabatic compression of the fluid), (ii) anisotropic stresses might arise, and finally (iii) velocity perturbations can experience viscous forces that dissipate kinetic energy. (For literature in this field we refer to Battye & Moss 2006, 2009; Mota et al. 2007; Calabrese et al. 2011; Ballesteros et al. 2012; Sapone & Majerotto 2012; Appleby, Linder & Weller 2013; Sapone et al. 2013; Dossett & Ishak 2013; Basse et al. 2014; Sawicki et al. 2013; Amendola et al. 2014; Chang & Xu 2014; Chang, Lu & Xu 2014; Cardona, Hollenstein & Kunz 2014; Pearson 2014; Ballesteros 2015). In addition, there can be a non-linear relation between pressure and density of a fluid, one example of which would be Chaplygin cosmologies (Bento, Bertolami & Sen 2002; Li & Xu 2014). Alternatively, a similar phenomenology could in principle be due to modifications in gravity rather than due to non-ideal fluids under general relativity (Kunz & Sapone 2007; Bertschinger & Zukin 2008; Silvestri 2009; Pogosian et al. 2010; Song et al. 2010; Leon & Saridakis 2011; Saltas & Kunz 2011; Baker, Ferreira & Skordis 2013; Boubekeur et al. 2014).

These modifications break homogeneity on small scales. They require corresponding fluid equations for their time evolution, as well couplings to local gravitational fields. The latter enable interaction between the dark energy fluid, the dark matter and the baryonic component. Commonly, one observes a difference between the two metric potentials in the case of non-zero sound speeds and equations of state unequal to -1. Such difference can be probed by photons, and is relative to the motion of non-relativistic objects such as galaxies, which are only sensitive to a single metric potential.

In this paper, we investigate cosmological perturbations with a non-ideal dark energy fluid and aim to forecast constraints on its speed of sound c_s and its viscosity from *Euclid*[1] (Laureijs 2009; Laureijs et al. 2011) and *Planck* (Planck Collaboration XVI 2014b; Planck Collaboration XIII 2015). Specifically, we consider tomographic weak gravitational lensing (Ayaita, Schäfer & Weber 2012), galaxy clustering (DeDeo, Caldwell & Steinhardt 2003; Takada 2006) and the integrated Sachs–Wolfe effect (Dossett & Ishak 2013; Soergel et al. 2015) as probes on the influence of non-ideal fluids on the statistics and the evolution of structures. The background expansion dynamics instead is given through the individual density parameters and the equation-of-state parameters, assuming that there is no energy exchange between the fluids.

Our work is complementary to that of Mota et al. (2007), Calabrese et al. (2011), Chang & Xu (2014), who used the same model to describe the evolution of anisotropic stress. Mota et al. (2007) and Chang & Xu (2014) computed constraints on it from the cosmic microwave background (CMB), the large-scale structure and Supernovae Type Ia, while Calabrese et al. (2011) forecasted errors from the CMB on the parameters of an early dark energy possessing anisotropic stress. It is also complementary to that of Amendola et al. (2014), Cardona et al. (2014) and Sawicki et al. (2013), who also put constraints on anisotropic dark energy, but used different models for its evolution.

Currently, there are no significant deviations from dark energy being a perfect fluid. See for instance the result by Bean & Doré (2004) who find $c_s^2 < 0.04$ at low significance from CMB data. Hence, tests whether dark energy is an ideal fluid will be the domain of future experiments. Quite generally, the sensitivity to non-ideal cosmic fluids requires their respective density to be large enough and their equation of state not to be too close to -1 for dark energy perturbations to be sufficiently strong (Erickson et al. 2002; Koivisto & Mota 2006; Ballesteros & Lesgourgues 2010; de Putter, Huterer & Linder 2010; Archidiacono, Lopez-Honorez & Mena 2014). At a first sight, it would appear that choosing a dark energy equation of state too far from the cosmological constant value is incompatible with present constraints (Planck Collaboration XIII 2015). However, when including extra parameters such as the speed of sound and viscosities in the fluid, constraints become much more loose (See e.g. Mota et al. 2007; Archidiacono et al. 2014).

This article is structured as follows. We develop the necessary perturbation equations for non-ideal dark energy fluids and a suitable parametrization in Section 2 and discuss cosmological probes in Section 3, before computing forecasts on non-ideal dark energy properties in Section 4. We summarize our results in Section 5. As regards the forecasts, let us remark that some of the authors are currently involved in a code comparison effort taking place within the *Euclid* Collaboration Forecast project. We want to stress then that some of the numbers in this paper might or might not change once agreement between different codes will be reached. The reference cosmological model is a spatially flat, dark-energy dominated model with the parameter choices $\{\Omega_m h^2, \Omega_b h^2, n_s, \Omega_m, w\} = \{0.142, 0.022, 0.96, 0.32, -0.8\}$. The first four correspond to the constraints from *Planck* (Planck Collaboration XVI 2014b) and *WMAP* polarization low-multipole likelihood (Bennett et al. 2013; Planck Collaboration XV 2014a), and they represent the present official baseline for *Euclid* forecasts. The dark energy equation-of-state parameter was instead set to a fiducial value of $w = -0.8$, in order for it to be sufficiently far from -1 (see discussion above). The amplitude of the primordial power spectrum was fixed to $A_s = 2.1 \times 10^{-9}$.

2 COSMOLOGY WITH NON-IDEAL FLUIDS

2.1 Expansion dynamics

Since we focus on late cosmological times, where dark matter and dark energy are dominating the energy density of the Universe, we can approximate the Hubble function $H(a) = \dot{a}/a$ with

$$H^2 = H_0^2 \left[\Omega_{m,0} a^{-3} + (1 - \Omega_{m,0}) a^{-3(1+w)}\right]. \quad (1)$$

Here, a is the scalefactor, $\Omega_{m,0}$ is the dark matter density parameter today, w is the equation of state of dark energy, which we assume to be constant, and H_0 is the Hubble parameter today. In addition, we do not consider global curvature. The comoving distance is defined as

$$\chi = c \int_a^1 \frac{da}{a^2 H(a)} \equiv \chi_H \int_a^1 \frac{da}{a^2 H(a)/H_0}, \quad (2)$$

with the Hubble distance $\chi_H = c/H_0 \simeq 2996.9\,\mathrm{Mpc}/h$. At the same time, this defines conformal time τ through $\chi = c\tau$. In the following, we will set $c = 1$.

2.2 Perturbations and their analytical solutions

If we consider a non-ideal fluid dark energy, characterized by a constant equation of state w, a speed of sound c_s, and an anisotropic stress component σ, we can write the evolution of σ as in Hu (1998):

$$\sigma' + \frac{3}{a}\sigma = \frac{8}{3}\frac{c_v^2}{(1+w)^2}\frac{V}{a^2 H}. \quad (3)$$

Here, the prime indicates derivative with respect to a and c_v^2 is called viscosity parameter, as it gives a measure of the fluid's viscosity. Indeed, equation (3) implies that when $c_v^2 = 0$, then the anisotropic

[1] http://www.euclid-ec.org/

stress component σ is also vanishing, while when e.g. $c_v^2 = 1/3$ the evolution of anisotropic stress for radiation up to the quadrupole is recovered.

To this equation, we add the first order perturbation equations for the density contrast δ and the velocity perturbation V

$$\delta' = 3(1+w)\phi' - \frac{V}{Ha^2} - 3\frac{1}{a}\left(\frac{\delta p}{\rho} - w\delta\right), \tag{4}$$

$$V' = -(1-3w)\frac{V}{a} + \frac{k^2}{Ha^2}\frac{\delta p}{\rho} + (1+w)\frac{k^2}{Ha^2}\psi + -(1+w)\frac{k^2}{Ha^2}\sigma, \tag{5}$$

where δp is the pressure perturbation, ρ is the dark energy density, ψ and ϕ are the metric perturbations in the Newtonian gauge, defined by the line element

$$\mathrm{d}s^2 = a^2\left[-(1+2\psi)\mathrm{d}\tau^2 + (1-2\phi)\mathrm{d}x_i\mathrm{d}x^i\right]. \tag{6}$$

Pressure perturbations are parametrized as

$$\delta p = c_s^2\rho\delta + \frac{3aH(c_s^2 - c_a^2)}{k^2}\rho V, \tag{7}$$

where $c_a^2 \equiv \dot{p}/\dot{\rho} = w$ is the adiabatic speed of sound for a fluid with constant equation of state. c_s^2 reduces to c_a^2 in the case of a perfect fluid, when no dissipative effects are present, which would otherwise lead to entropic perturbations (Bean & Doré 2004).

In order to close the differential equation system, one needs to include the Poisson equation

$$k^2\phi = -4\pi G a^2\sum_i \rho_i\left(\delta_i + \frac{3aH}{k^2}V_i\right) = -4\pi G a^2\sum_i \rho_i\Delta_i, \tag{8}$$

(where the sum runs over all clustering fluids, G is the Newton constant, and in the last equality we have defined the gauge-invariant density perturbation of the ith fluid, $\Delta_i \equiv \delta_i + 3aHV_i/k^2$) and the fourth Einstein equation

$$k^2(\phi - \psi) = 12\pi G a^2(1+w)\rho\sigma \tag{9}$$

$$= \frac{9}{2}H_0^2(1-\Omega_{m,0})a^{-(1+3w)}(1+w)\sigma \equiv B(a)\sigma. \tag{10}$$

In Sapone & Majerotto (2012) the following analytical solutions for δ, V and σ were found for the matter dominated era:

$$\delta = \frac{3(1+w)^2}{3c_s^2(1+w) + 8\left(c_s^2 - w\right)c_v^2}\frac{\phi_0}{k^2}, \tag{11}$$

$$V = -\frac{9(1+w)^2\left(c_s^2 - w\right)}{3c_s^2(1+w) + 8c_v^2(c_s^2 - w)}H_0\sqrt{\Omega_m}\frac{\phi_0}{\sqrt{a}k^2}, = -3aH\left(c_s^2 - w\right)\delta, \tag{12}$$

$$\sigma = -\frac{8c_v^2\left(c_s^2 - w\right)}{3c_s^2(1+w) + 8(c_s^2 - w)c_v^2}\frac{\phi_0}{k^2}, \tag{13}$$

where $k^2\phi \simeq -\phi_0$. The latter is valid strictly only during matter domination and while neglecting dark energy perturbations. Nevertheless, the validity of this approximation extends to redshifts very close to today's z, as can be seen from fig. 1 of Sapone & Majerotto (2012).

As found in Sapone & Majerotto (2012), to which we refer for further detail on the analytic solutions, the relevant quantity is the effective sound speed

$$c_{eff}^2 = c_s^2 + \frac{8}{3}c_v^2\frac{c_s^2 - w}{1+w}, \tag{14}$$

as equations (11)–(13) can be rewritten in terms of it. This means that the sound speed and the viscosity have a similar damping effect on density and velocity perturbations (as also noticed in Mota et al. 2007; Calabrese et al. 2011). It is interesting to notice that the effect of c_v^2 is enhanced with respect to that of c_s^2 by a factor of $8(c_s^2 - w)/[3(1+w)]$, which is $\sim$10 if $w \sim -0.8$ and c_s^2 is very small. A relative large w and very small c_s^2 are precisely the cases where a viscosity can be observed best, as will be shown in the following sections. Moreover c_{eff}^2 is bounded by the case of a cosmological constant, as equation (11) diverges for $w = -1$.

2.3 Observable parameters

To understand how the viscosity affects the physical observables, it is useful to introduce the clustering parameter Q and the anisotropy parameter η. These were defined in Amendola, Kunz & Sapone (2008) and computed in the case of viscous dark energy in Sapone & Majerotto (2012).

Q parametrizes the deviation from a purely matter-dominated Newtonian potential and is given by (see Sapone & Majerotto 2012)

$$Q - 1 \equiv \frac{\rho\Delta}{\rho_m\Delta_m} = \frac{1-\Omega_{m,0}}{\Omega_{m,0}}(1+w)\frac{a^{-3w}}{1 - 3w + \frac{2k^2a}{3H_0^2\Omega_{m,0}}c_{eff}^2} = Q_0\frac{a^{-3w}}{1+\alpha a}, \tag{15}$$

where $\alpha = 2k^2c_{eff}^2/[(3H_0^2\Omega_{m,0})(1-3w)]$ and $Q_0 = (1+w)(1-\Omega_{m,0})/[\Omega_{m,0}(1-3w)]$.

The anisotropy parameter is then given by

$$\eta \equiv \frac{\psi}{\phi} - 1 = -\frac{9}{2}H_0^2(1-\Omega_{m,0})(1+w)\frac{a^{-1-3w}}{k^2Q}\left(1 - \frac{c_s^2}{c_{eff}^2}\right). \tag{16}$$

This is non-zero only when anisotropic stress is present and the metric perturbations ϕ and ψ are different.

Let us finally define the parameter Σ (Amendola et al. 2008) as

$$\Sigma = \left(1 + \frac{1}{2}\eta\right)Q. \tag{17}$$

This is useful because it represents the deviation of the weak lensing potential $\Phi = \psi + \phi$ from its behaviour in the case of no dark energy perturbations. It is important to remark that for all our forecasts we used the numerical solutions to equations (3)–(5) and (8)–(9) computed with a modified version of the CAMB code[2] (Lewis, Challinor & Lasenby 2000), and not their analytic approximations, equations (11)–(13). We did use instead the analytical expression for the Q and Σ parameters. These approximate very well their numerical counterparts up to redshifts very close to 0, as shown in figs 3 and 4 of Sapone & Majerotto (2012)

[2] http://camb.info

3 COSMOLOGICAL PROBES

In Sapone et al. (2013), we forecasted constraints to the viscosity parameter and the sound speed from the *Euclid* galaxy clustering and weak lensing surveys. Here, we aim to complete the picture by adding to the latter the constraints from the iSW tomography signal obtained by cross-correlating galaxies mapped by the *Euclid* photometric instrument with the *Planck* temperature map. This provides a combination of all major probes of cosmic structure formation, which draw their sensitivity from the growth rate and interactions between fluids, from the shape of the initial perturbations and from the expansion history.

The *Euclid* survey is a mission of the ESA Cosmic Vision programme that will be launched in 2020, and will perform both a photometric and a spectroscopic survey, the first aiming mainly at measuring weak lensing while the second at measuring the galaxy power spectrum. The *Planck* satellite is also a mission of ESA Cosmic Vision programme, *which mapped* the CMB fluctuations with unprecedented precision and control of systematic effects.

To perform our forecasts, we use the Fisher matrix (Tegmark et al. 1997), which quantifies the decrease in likelihood if a model parameter θ_α moves away from the fiducial value, and can be computed for a local Gaussian approximation to the likelihood $\mathcal{L} \propto \exp(-\chi^2/2)$. In our forecasts we assume the official *Euclid* specifications, that can be found in Laureijs et al. (2011). The fiducial cosmological parameters correspond to the 2013 *Planck* measurements (Planck Collaboration XVI 2014b), except for the value of w, for which we assume $w = -0.8$, in order for the effects to be more clearly visible (as done in Sapone & Majerotto 2012; Sapone et al. 2013) and of course except for the values of c_s^2 and c_v^2.

In the following, we will describe the iSW tomography signal and give a short summary on the signal coming from weak lensing and the galaxy power spectrum from spectroscopy.

3.1 iSW signal

When a CMB photon moves into a time-evolving metric such as that of equation (6) the unbalance between the blueshift experienced at the entrance and the redshift experienced at the exit of its varying potential well originates a perturbation ζ in the CMB temperature $T_{\rm CMB}$ given by (Sachs & Wolfe 1967),

$$\zeta = \frac{\Delta T}{T_{\rm CMB}} \equiv \int \mathrm{d}\tau \left(\frac{\partial \phi}{\partial \tau} + \frac{\partial \psi}{\partial \tau}\right) = \int_0^{\chi_H} \mathrm{d}\chi\, a^2 H \frac{\partial \Phi}{\partial a}, \qquad (18)$$

where χ is the comoving distance (see equation 2) and Φ is the weak lensing potential.

In the case of pure matter domination, $\Phi = $ const, hence the iSW effect vanishes, while in presence of any fluid with $w \neq 0$ the temperature fluctuation ζ will be non-zero. This is why the late iSW is particularly interesting to us, as it is originated by the appearing of dark energy and it is an independent proof of its existence (first detected by Boughn & Crittenden 2004; Giannantonio et al. 2012, for an updated measurement).

Let us now compute the term inside the integral, passing to Fourier space, and in the case of viscous dark energy (see also Schaefer 2009; Sapone & Majerotto 2012):

$$\frac{\partial \Phi}{\partial a} = -\frac{3}{2}\frac{H_0^2 \Omega_{\rm m,0}}{a k^2}\left\{\Sigma(a,k)\,\Delta_{\rm m}'(a,k) + \Sigma'(a,k)\,\Delta_{\rm m}(a,k) - \frac{1}{a}\Sigma(a,k)\,\Delta_{\rm m}(a,k)\right\}. \qquad (19)$$

It is possible to see from this expression that anisotropic perturbations enter the iSW effect in two ways: by modifying $\Delta_{\rm m}$ and through the additional presence of Σ and Σ'. At linear order, it is possible to isolate today's $\Delta_{\rm m}$ from its time evolution:

$$\Delta_{\rm m}(a,k) = aG(a,k)\,\Delta_{\rm m,0}(k), \qquad (20)$$

where $\Delta_{\rm m,0}(k) \equiv \Delta_{\rm m}(a=1,k)$. We write hence equation (19) as:

$$\frac{\partial \Phi}{\partial a} = -\frac{3}{2}\frac{H_0^2 \Omega_{\rm m,0}}{k^2}\frac{\partial}{\partial a}\{G(a,k)\,\Sigma(a,k)\}\Delta_{\rm m,0}(k), \qquad (21)$$

and equation (18) reads now

$$\zeta = \int_0^{\chi_H} \mathrm{d}\chi\; W_\zeta(\chi)\,\Delta_{\rm m,0}(k) \qquad (22)$$

where the weighting function $W_\zeta(\chi)$ is

$$W_\zeta(\chi) = \frac{3}{2}\frac{H_0^2 \Omega_{\rm m,0}}{k^2} a^2 H \frac{\partial}{\partial a}\{G(a,k)\,\Sigma(a,k)\}. \qquad (23)$$

Since the iSW is a secondary effect of the CMB (Rees & Sciama 1968), it can be *extracted* through cross-correlation *of the CMB temperature fluctuations* to the galaxy density (Crittenden & Turok 1996). Let us hence write the galaxy density obtained through imaging surveys, in order to compute its cross-correlation with the iSW. The line-of-sight projected galaxy density γ is given by (Smail et al. 1995)

$$\gamma = \int_0^{\chi_H} \mathrm{d}\chi\; D(z)\frac{\mathrm{d}z}{\mathrm{d}\chi} b(\chi) G(\chi)\delta(z) \qquad (24)$$

being $D(z)$ the galaxy distribution defined as

$$D(z) = \left(\frac{z}{z_0}\right)^2 \exp\left[-\left(\frac{z}{z_0}\right)^{\beta_D}\right], \qquad (25)$$

where the fiducial parameters β_D and z_0 depend on the imaging survey considered. In the case of *Euclid*, they are $\beta_D = 3/2$, $z_0 = z_{\rm mean}/\sqrt{2}$, and $z_{\rm mean} = 0.9$ (Laureijs et al. 2011).

Even though the signal from the iSW increases noticeably when cross-correlating it with the galaxy density field, both the cross-correlation spectrum and the galaxy spectrum are line-of-sight integrated quantities, hence much information may be lost. For this reason, we decide to use iSW tomography (Douspis et al. 2008; Ho et al. 2008; Juergens & Schaefer 2012). In particular we divide the whole galaxy sample into 5 bins with equal number of galaxies (in order to match with the binning used by official *Euclid* documents for weak lensing tomography). To do this, we replace the galaxy distribution function $D(z)$, equation (25) in γ, equation (24), with the radial distribution function of galaxies in the ith bin $D_i(z)$. The latter is obtained by binning the overall distribution $D(z)$ and convolving it with the photometric redshift distribution function (Amendola et al. 2008).

We are finally able to write our observable, i.e. the iSW-galaxy cross-correlation spectrum in the i-th redshift bin, along with the iSW-auto correlation spectrum $C_{\zeta\zeta}(\ell)$ and the galaxy–galaxy auto correlation spectrum $C_{\gamma\gamma,ij}(\ell)$ of the ij-bins, by applying a Limber projection (Limber 1954) in the flat-sky approximation:

$$C_{\zeta\gamma,i}(\ell) = \int_0^{\chi_H} \frac{\mathrm{d}\chi}{\chi^2}\, W_\zeta(\chi) W_{\gamma,i}(\chi)\, P_{\Delta\Delta}(k = \ell/\chi), \qquad (26)$$

$$C_{\zeta\zeta}(\ell) = \int_0^{\chi_H} \frac{\mathrm{d}\chi}{\chi^2}\, W_\zeta^2(\chi)\; P_{\Delta\Delta}(k = \ell/\chi) \qquad (27)$$

$$C_{\gamma\gamma,ij}(\ell) = \int_0^{\chi_H} \frac{\mathrm{d}\chi}{\chi^2}\, W_{\gamma,i}(\chi) W_{\gamma,j}(\chi)\, P_{\Delta\Delta}(k = \ell/\chi) \qquad (28)$$

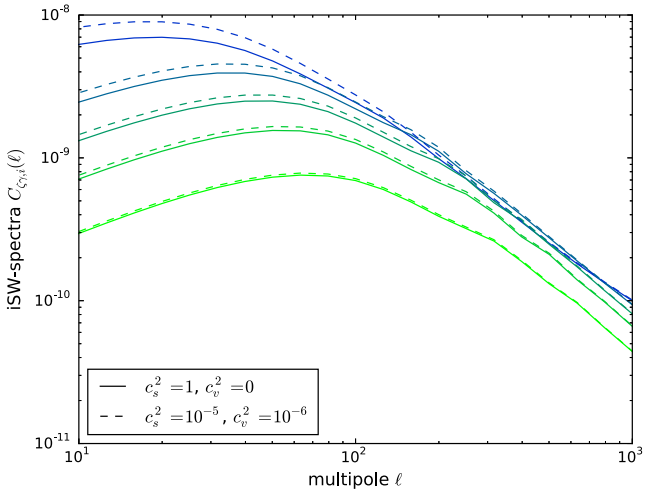

Figure 1. Tomographic iSW-spectra $C_{\zeta\gamma,i}(\ell)$ for two dark energy models: $c_s^2 = 1$ and $c_v^2 = 0$ as well as $c_s^2 = 10^{-5}$, $c_v^2 = 10^{-6}$. Blue to light green lines (top to bottom) correspond to redshifts z in the intervals [0.01 − 0.5595] (blue), [0.5595 − 0.7871], [0.7871 − 1.0165], [1.0165 − 1.3184] and finally [1.3184 − 2.5] (green).

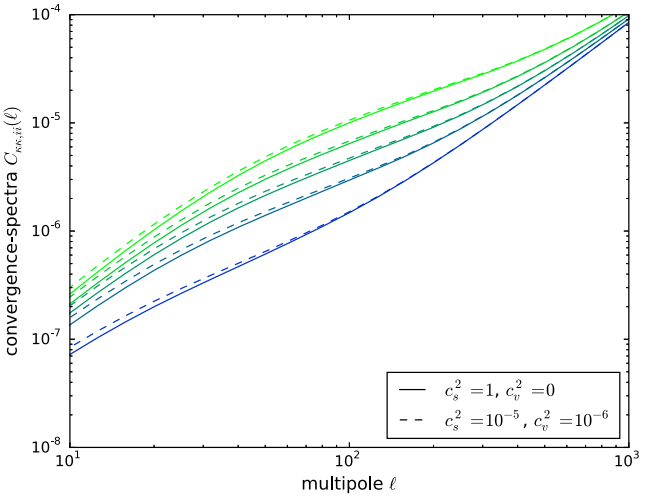

Figure 2. Tomographic weak lensing spectra $C_{\kappa\kappa,ii}(\ell)$ for two dark energy models, $c_s = 1$ and $c_v = 1$ as well as $c_s = 10^{-5}$, $c_v = 10^{-6}$, both including the shape noise term. Blue to light green lines (bottom to top) correspond to the same redshift binning as in Fig. 1: [0.01 − 0.5595] (blue), [0.5595 − 0.7871], [0.7871 − 1.0165], [1.0165 − 1.3184] and finally [1.3184 − 2.5] (green).

Here $\bar{P}_{\Delta\Delta}(k)$ is the linear matter power spectrum today, and the galaxy weighting function of the ith bin $W_{\gamma,i}(\chi)$ is

$$W_{\gamma,i}(\chi) = D_i(z)\frac{\mathrm{d}z}{\mathrm{d}\chi}b(\chi)G(\chi). \tag{29}$$

$C_{\zeta\zeta}(\ell)$ and $C_{\gamma\gamma,ij}(\ell)$ have been computed because they are needed in order to estimate statistical errors of $C_{\zeta\gamma,i}(\ell)$. The tomographic iSW spectra $C_{\zeta\gamma,i}(\ell)$ are shown in Fig. 1 for two fiducial models: a standard dark energy model with $c_s^2 = 1$ and $c_v^2 = 0$ (solid lines) and a model with viscosity: $c_s^2 = 10^{-5}$ and $c_v^2 = 10^{-6}$ (dashed lines). The colour shading indicates the redshift bin for which $C_{\zeta\gamma,i}(\ell)$ was evaluated. The iSW effect is a large-scale effect originating from low redshift, as the influence of dark energy on the growth of gravitational potentials in the large-scale structure is strongest. The effect of dark energy viscosity and small sound speed is strongest on large scales as well (see also Sapone & Majerotto 2012), and affects a wide range of multipoles. Keeping all cosmological parameters fixed, dark energy viscosity would increase the amplitude of the iSW effect by up to 25 per cent on large angular scales and at low redshift. This sensitivity of the spectra at low multipoles is fortunate because these scales can be well probed with the iSW effect.

3.2 Weak lensing

To the iSW tomography signal we add the weak lensing tomographic signal (Hu 1999, 2002; Heavens 2003; Jain & Taylor 2003), coming from the same photometric survey as γ and using the same redshift bins. Here, we only give the main equation expressing the weak lensing power spectrum, which is used for our forecasts, and refer to Sapone et al. (2013) for further details.

In presence of anisotropic stress, the weak lensing convergence power spectrum is given by (Hu 1999, 2002; Jain & Taylor 2003; Hu & Jain 2004)

$$C_{\kappa,ij}(\ell) = \int_0^{\chi_H}\frac{\mathrm{d}\chi}{\chi^2}\,W_{\kappa,i}(\chi)W_{\kappa,j}(\chi)\,\Sigma^2\,P_{\rm NL}(k=\ell/\chi,\chi). \tag{30}$$

where the subscript ij refers to the redshift bins around z_i and z_j, with

$$W_{\kappa,i}(\chi) = \frac{3\Omega_{\rm m}}{2\chi_H^2}\frac{F_i(\chi)}{a}\chi \tag{31}$$

$$F_i(\chi) = \int_\chi^{\chi_H}\mathrm{d}\chi' n(\chi')\,D_i(\chi')\,\frac{\chi'-\chi}{\chi'} \tag{32}$$

and where D_i is the same tomographic distribution function of galaxies used for the iSW effect. While tomography in general greatly reduces statistical errors, the actual shape of the choice of the binning does not affect results in a serious way, although in principle there is room for optimization (Schäfer & Heisenberg 2012).

In Fig. 2 we show the tomographic weak lensing spectra $C_{\kappa,ii}(\ell)$ for the same models and the same redshifts as in Fig. 1. As for iSW, the effect of viscosity is detected at large scales and for a large range of scales (but smaller than for iSW). Instead, contrarily to iSW, here the sensitivity to viscosity is stronger at higher redshift. This is because the efficiency of weak lensing is higher for longer light paths.

In principle it is also possible to define a cross-spectrum of weak lensing and iSW, $C_{\kappa\zeta,i}(\ell)$, and of weak lensing and galaxy distribution, $C_{\kappa\gamma,i}(\ell)$, but both these spectra are subdominant with respect to $C_{\zeta\gamma}(\ell)$. This is because the weak lensing convergence signal comes from the distortion of the light path at redshifts intermediate between us and the galaxies mapped by the imaging survey, while the iSW signal originates precisely at the same redshifts where the galaxies are. We have tested this fact by computing the signal to noise-ratio for measuring $C_{\zeta\kappa,i}(\ell)$ and found it much smaller than that of $C_{\zeta\gamma,i}(\ell)$.

3.3 Spectroscopic galaxy power spectrum

To the iSW and weak lensing measurements, both measured through photometric observations, we add data coming from the power spectrum of spectroscopically observed galaxies. Here, we only show the expression of the observed power spectrum, which is needed in

order to compute our forecasts, and refer again the reader to Sapone et al. (2013) for further detail.

Following Seo & Eisenstein (2003) we write the observed galaxy power spectrum as

$$P^{\rm spec}_{\gamma\gamma}(z, k_r, \mu_r) = \frac{D^2_{Ar}(z)H(z)}{D^2_A(z)H_r(z)} G^2(z,k) b(z)^2 \left(1+\beta\mu^2\right)^2 P_{0r}(k) + P_{\rm shot}, \quad (33)$$

where the subscript r refers to the reference (or fiducial) cosmological model.

Here $P_{\rm shot}$ is a scale-independent offset due to imperfect removal of shot-noise, $\mu = \boldsymbol{k}\cdot\hat{\boldsymbol{r}}/k$, is the cosine of the angle of the wave mode with respect to the line of sight pointing into the direction $\hat{\boldsymbol{r}}$, P_{0r} is the fiducial matter power spectrum evaluated at redshift zero, $G(z, k)$ is the linear growth factor of the matter perturbations, $b(z)$ is the bias factor and $D_A(z)$ is the angular diameter distance. The wavenumber k and μ have also to be written in terms of the fiducial cosmology (see Seo & Eisenstein 2003; Amendola, Quercellini & Giallongo 2005; Sapone & Amendola 2007, for more details). The fiducial bias used can be found in Orsi et al. (2010), who derived their results by using a semi-analytical model of galaxy formation. The matter power spectrum has been computed with a modified version of the CAMB code accounting for anisotropies.

4 STATISTICAL ERRORS FORECASTS

In this section, we estimate marginalized statistical errors on the sound speed and viscosity parameters $c_{\rm s}^2$ and $c_{\rm v}^2$ through the Fisher-matrix formalism (Tegmark et al. 1997), which assumes a Gaussian likelihood and unbiased measurements.

4.1 iSW Fisher matrix

The sensitivity of line of sight-integrating effects can be boosted by subdividing the galaxy population into redshift bins. For the iSW effect, this was first carried out successfully by Ho et al. (2008), and systematically investigated by Juergens & Schaefer (2012).

The Fisher matrix of the iSW effect follows directly from the variance of the spectrum estimates,

$$F^{\rm iSW}_{\alpha\beta} = \sum_\ell \frac{\partial \bar{C}_{\zeta\gamma,i}(\ell)}{\partial\theta_\alpha} {\rm Cov}^{-1}_{ij}(\ell) \frac{\partial \bar{C}_{\zeta\gamma,j}(\ell)}{\partial\theta_\beta}. \quad (34)$$

Here the sum runs from $\ell = 5$ to $\ell = 300$,[3] θ_α are the cosmological parameters, ${\rm Cov}_{ij}(\ell)$ is the covariance of the spectrum $\bar{C}_{\zeta\gamma,i}(\ell)$ and is given by

$${\rm Cov}_{ij}(\ell) = \frac{1}{2\ell+1}\frac{1}{f_{\rm sky}}\left[\bar{C}_{\zeta\gamma,i}\bar{C}_{\zeta\gamma,j}(\ell) + \bar{C}_{\zeta\zeta}(\ell)\bar{C}_{\gamma\gamma,ij}(\ell)\right], \quad (35)$$

and where quantities with the bar represent the estimate of the signal, including intrinsic CMB fluctuations, instrumental noise and the beam of the CMB experiment as noise sources:

$$\bar{C}_{\zeta\gamma,i}(\ell) = C_{\zeta\gamma,i}(\ell) \quad (36)$$

$$\bar{C}_{\zeta\zeta}(\ell) = C_{\zeta\zeta}(\ell) + C_{\rm CMB}(\ell) + w_T^{-1}B^{-2}(\ell) \quad (37)$$

[3] The integration range for the iSW effect as well as the details of instrumental noise and angular resolution are not very important, as most of the signal is at low ℓ below $\ell \sim 100$, due to the large cosmic variance provided by the primary CMB fluctuations, which is the largest source of noise.

$$\bar{C}_{\gamma\gamma,ij}(\ell) = C_{\gamma\gamma,ij}(\ell) + \frac{\delta_{ij}}{n_i} \quad (38)$$

For *Planck*'s noise levels, $w_T^{-1} = (0.012\mu{\rm K})^2$ has been used (Tauber et al. 2006) and the beam was assumed to be Gaussian, $B^{-2}(\ell) = (2\times10^{-8})^2 \exp\left[\Delta\theta^2\ell(\ell+1)\right]$, with FWHM width of $\Delta\theta = 7.1$ arcmin, corresponding to channels of *Planck* closest to the CMB maximum at ∼160 GHz. n_i is the number of galaxies per steradian in the tomography bin i. We assume uncorrelated noise terms, and as a consequence the cross-spectra $C_{\zeta\gamma,i}(\ell)$ are unbiased estimates of the actual spectra, see equation (36). The spectrum $C_{\rm CMB}(\ell)$ of the CMB primary anisotropies from *Planck* has been computed with the CAMB code.

4.2 Weak lensing Fisher matrix

The Fisher matrix for weak lensing is given by

$$F^{\rm WL}_{\alpha\beta} = f_{\rm sky}\sum_\ell \frac{(2\ell+1)}{2}\frac{\partial C_{\kappa\kappa,ij}(\ell)}{\partial\theta_\alpha}\bar{C}^{-1}_{jk}(\ell)\frac{\partial C_{\kappa\kappa,km}(\ell)}{\partial\theta_\beta}\bar{C}^{-1}_{mi}(\ell) \quad (39)$$

where the sum runs from $\ell = 5$ to 5000, (as from the official *Euclid* prescriptions, see Laureijs et al. 2011), and where the sum over repeated indices is implied. We added a Poissonian shape noise term to the weak lensing spectra,

$$\bar{C}_{\kappa\kappa,ij}(\ell) = C_{\kappa\kappa,ij}(\ell) + \delta_{ij}\frac{\langle\gamma^{1/2}_{\rm int}\rangle}{n_i}, \quad (40)$$

$\gamma_{\rm int}$ is the rms intrinsic shear (here, we assume $\langle\gamma^{1/2}_{\rm int}\rangle$=0.22) and n_i is the number of galaxies per steradians belonging to the ith bin. We assume a Gaussian shape of the covariance while noting that non-Gaussian contribution can have a strong influence on the derived forecasts (Takada & Jain 2009).

4.3 Spectroscopic galaxy distribution Fisher matrix

The galaxy power spectrum Fisher matrix is given by (Seo & Eisenstein 2003)

$$F^{\rm GC}_{\alpha\beta} = \int_{k_{\rm min}}^{k_{\rm max}} \frac{k^2{\rm d}k}{4\pi^2}\frac{\partial \ln P^{\rm spec}_{\gamma\gamma}(z;k,\mu)}{\partial\theta_\alpha}\frac{\partial \ln P^{\rm spec}_{\gamma\gamma}(z;k,\mu)}{\partial\theta_\beta} \times V_{\rm eff}, \quad (41)$$

where GC stays for galaxy clustering, the observed galaxy power spectrum $P^{\rm spec}_{\gamma\gamma}$ is given by equation (33), the derivatives are evaluated at the parameter values of the fiducial model. $k_{\rm min} = 0.001$ and $k_{\rm max}$ is such that the rms amplitude of the fluctuations at the corresponding scale $R_{\rm max} = 2\pi/k_{\rm max}$ is $\sigma^2(R_{\rm max}) = 0.25$, with an additional cut at $k_{\rm max} = 0.2\,h$/Mpc, in order to remain in the linear regime. $V_{\rm eff}$ is the effective volume of the survey, given by

$$V_{\rm eff} \simeq \left(\frac{\bar{n}\,P^{\rm spec}_{\gamma\gamma}(k,\mu)}{\bar{n}\,P^{\rm spec}_{\gamma\gamma}(k,\mu)+1}\right)^2 V_{\rm survey}. \quad (42)$$

The latter equation holds for an average comoving number density $\bar{n}$. The number densities and further fiducial *Euclid* specifications can be found in Laureijs et al. (2011) and Majerotto et al. (2012).

4.4 Forecasts

We computed forecasts on the measurement of $c_{\rm s}^2$ and $c_{\rm v}^2$ for a wide range of fiducial values, in order to capture the parameter determining capability of both experiments for a previously unknown set of

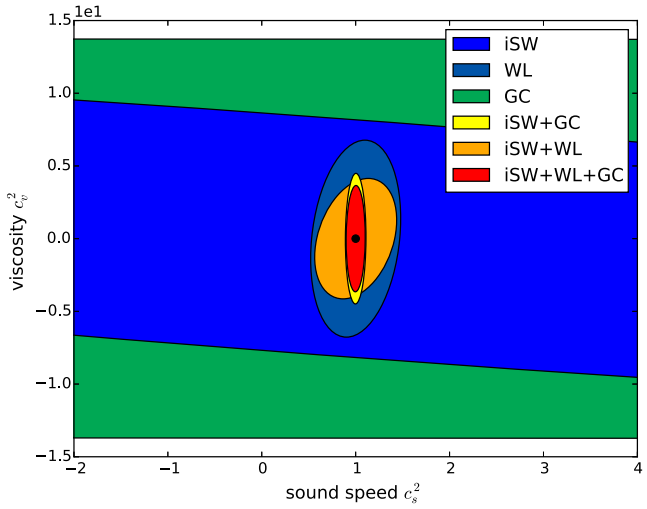

Figure 3. Forecasted 1σ constraints on c_s^2 and c_v^2 for individual probes and all possible combinations, for the fiducial choice $c_s^2 = 1$ and $c_v^2 = 0$.

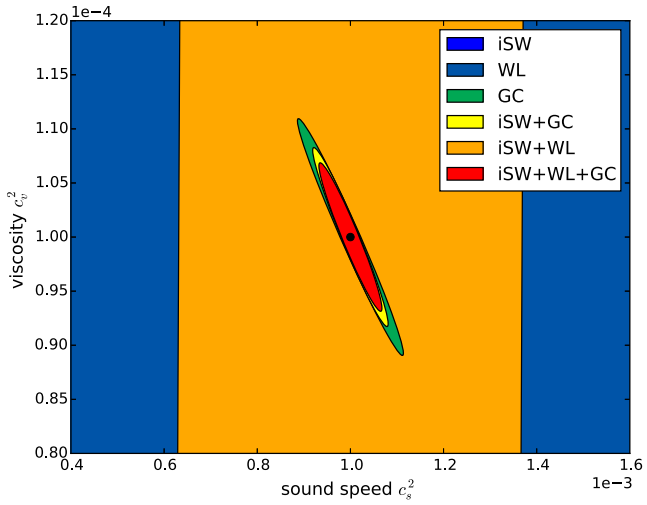

Figure 4. Forecasted 1σ constraints on c_s^2 and c_v^2 for individual probes and all possible combinations, for the fiducial choice $c_s^2 = 10^{-3}$ and $c_v^2 = 10^{-4}$.

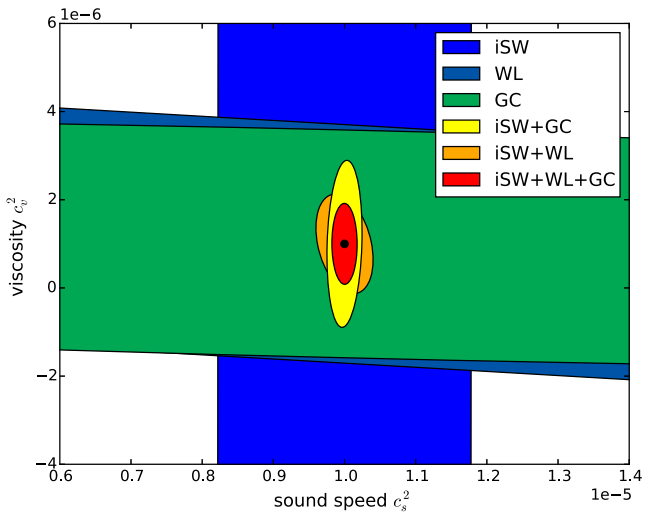

Figure 5. Forecasted 1σ-constraints on c_s^2 and c_v^2 for individual probes and all possible combinations, for the fiducial choice $c_s^2 = 10^{-5}$ and $c_v^2 = 10^{-6}$.

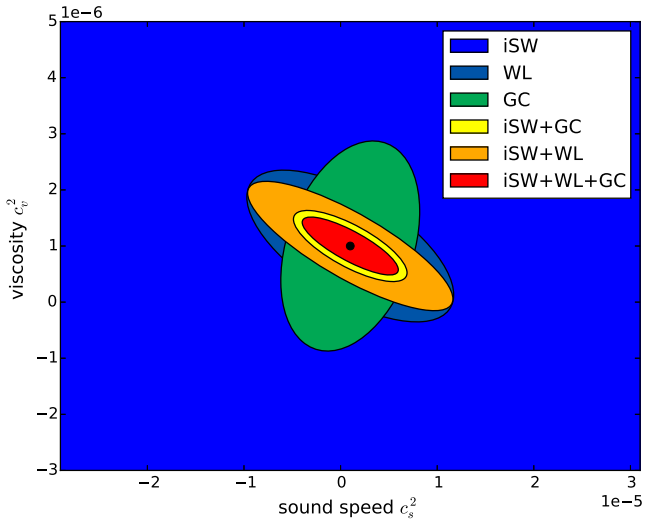

Figure 6. Forecasted 1σ constraints on c_s^2 and c_v^2 for individual probes and all possible combinations, for the fiducial choice $c_s^2 = 10^{-6}$ and $c_v^2 = 10^{-6}$.

parameters. The probes are assumed to be uncorrelated as discussed above, hence their Fisher matrices add,

$$F_{\alpha\beta} = F_{\alpha\beta}^{\rm GC} + F_{\alpha\beta}^{\rm WL} + F_{\alpha\beta}^{\rm iSW}, \tag{43}$$

and we derive confidence contours on c_s^2 and c_v^2 and individual errors from this combined Fisher matrix, marginalizing over all other five parameters considered in this analysis. $F_{\alpha\beta}^{\rm GC}$ has been further marginalized over $P_{\rm shot}$, while the galaxy bias has been kept fixed to the fiducial values of Orsi et al. (2010) (see Section 3.3).

Our forecasts on the following fiducial models: $\{c_s^2, c_v^2\} = \{1, 0\}$, $\{10^{-3}, 10^{-4}\}$, $\{10^{-5}, 10^{-6}\}$ and $\{10^{-6}, 10^{-6}\}$ are shown in Figs 3, 4, 5 and 6, respectively. The first model corresponds to the case of simple scalar field dark energy, while the following two pairs of fiducial models were chosen such that $c_s^2 = 10\,c_v^2$. This is because, as mentioned previously in Section 2.2, the relevant quantity is the effective sound speed, and the effect of c_v^2 in it is $\sim$10 times stronger than that of c_s^2 when $w = -0.8$ because of the factor multiplying c_v^2 in equation (14). The last model, also having small c_s^2 and c_v^2, does not verify the latter relation, and has been chosen in order to be compared to previous work (Sapone et al. 2013) and to the similar case $\{c_s^2, c_v^2\} = \{10^{-5}, 10^{-6}\}$.

In all plots, iSW constraints are shown in blue, weak lensing ones in dark blue, GC ones in green, combined iSW-GC ones in yellow, combined iSW-weak lensing ones in orange, and combined iSW-GC-weak lensing ones in red.

From Figs 3–6 it is clear that the results depend very much on the chosen fiducial model. A common feature is that iSW on its own does not provide very strong constraints. In particular (see also Table 1), c_v^2 is quite badly constrained, with relative errors ranging between 6.1×10^4 and 1.1×10^5, while relative errors on c_s^2 are much smaller: between 1.1×10^{-1} and 1.4×10. This was to be expected since the iSW effect alone has a rather small signal strength of about 5σ for cross-correlating the CMB with the *Euclid* galaxy sample (Douspis et al. 2008).

Table 1. 1σ errors on the parameters c_s^2 and c_v^2 from iSW, weak lensing and GC alone, from the combination of iSW and WL, iSW and GC, GC and WL, and from all three data sets. For the case $c_v^2 = 0$ the absolute error $\sigma_{c_v^2}$ is given.

	c_s^2	c_v^2	$\sigma_{c_s^2}$	$\sigma_{c_v^2}$
iSW	1	0	1.4×10	8.6
	10^{-3}	10^{-4}	1.4×10^{-2}	6.1
	10^{-5}	10^{-6}	1.4×10^{-6}	1.1×10^{-1}
	10^{-6}	10^{-6}	4.0×10^{-4}	4.4×10^{-5}
WL	1	0	3.2×10^{-1}	4.5
	10^{-3}	10^{-4}	1.6×10^{-1}	1.4×10^{-2}
	10^{-5}	10^{-6}	3.7×10^{-4}	3.5×10^{-5}
	10^{-6}	10^{-6}	7.1×10^{-6}	8.9×10^{-7}
GC	1	0	1.1×10^{2}	9.1
	10^{-3}	10^{-4}	7.5×10^{-5}	7.2×10^{-6}
	10^{-5}	10^{-6}	2.2×10^{-5}	1.9×10^{-6}
	10^{-6}	10^{-6}	4.7×10^{-6}	1.2×10^{-6}
iSW+WL	1	0	2.9×10^{-1}	2.7
	10^{-3}	10^{-4}	2.5×10^{-4}	5.6×10^{-4}
	10^{-5}	10^{-6}	2.6×10^{-7}	7.5×10^{-7}
	10^{-6}	10^{-6}	7.0×10^{-6}	7.6×10^{-7}
iSW+GC	1	0	7.2×10^{-2}	3.0
	10^{-3}	10^{-4}	5.3×10^{-5}	5.5×10^{-6}
	10^{-5}	10^{-6}	1.6×10^{-7}	1.2×10^{-6}
	10^{-6}	10^{-6}	3.9×10^{-6}	4.2×10^{-7}
GC+WL	1	0	6.7×10^{-2}	3.7
	10^{-3}	10^{-4}	7.4×10^{-5}	7.1×10^{-6}
	10^{-5}	10^{-6}	1.9×10^{-5}	1.7×10^{-6}
	10^{-6}	10^{-6}	3.5×10^{-6}	4.8×10^{-7}
All	1	0	6.7×10^{-2}	2.4
	10^{-3}	10^{-4}	4.5×10^{-5}	4.5×10^{-6}
	10^{-5}	10^{-6}	1.2×10^{-7}	6.1×10^{-7}
	10^{-6}	10^{-6}	3.3×10^{-6}	3.4×10^{-7}

Weak lensing constraints[4] are much stronger than iSW ones in the case of a fiducial scalar field dark energy, but become progressively comparable to them when the fiducial c_s^2 and c_v^2 become smaller, with the exception of the case $c_s^2 = c_v^2 = 10^{-6}$.

Even though both iSW and weak lensing do not give very strong constraints on sound speed and viscosity (see also Table 1), it is very interesting to notice that the two data sets complement each other very well. This is especially true for the case $c_s^2 = 10^{-5}$ and $c_v^2 = 10^{-6}$, represented in Fig. 5, where the blue ellipses, which indicate errors from iSW, have a very different degeneration direction with respect to the dark blue contours, corresponding to errors from weak lensing, but are comparable to them in size. Therefore the resulting combined errors are much smaller than those from a single data set. In particular, the iSW effect gives better constraints on the sound speed and weak lensing on the viscosity parameter. Also in the cases of Figs 3, 4 and 6 there is a visible but small improvement when adding iSW to the other data sets. The reason for this is that iSW's sensitivity to c_s^2 and c_v^2 is comparable to that of GC and WL, but its sensitivity to all other parameters is much less than that of the other observables. This can be seen by comparing the Fisher matrix elements, and it is demonstrated in the example of Fig. 7. Here we show how the error on c_s^2 from GC, for the fiducial model with

[4] With respect to Sapone et al. (2013) we have improved the estimation of P_{NL} by using the full CAMB output instead of an analytical approximation to it.

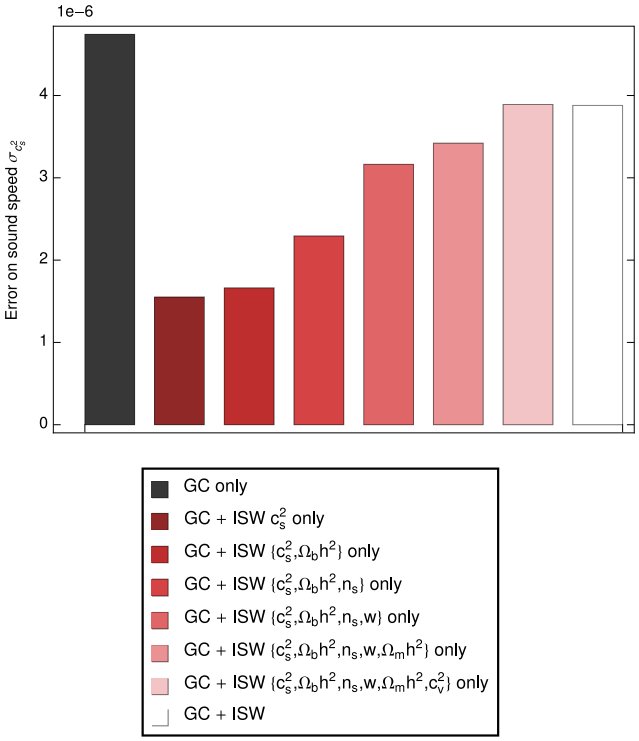

Figure 7. Errors on c_s^2, for the fiducial model with $c_s^2 = 10^{-6}$ and $c_v^2 = 10^{-6}$, from the GC Fisher matrix joined with progressively larger iSW sub-matrices. The first bar on the left corresponds to $\sigma_{c_s^2}$ from GC only, while the last one on the right corresponds to $\sigma_{c_s^2}$ from joint GC-iSW data. The second bar from the left corresponds to adding to GC only the $c_s^2 - c_s^2$ element of the iSW Fisher, the third to adding the $c_s^2 - \Omega_b h^2$ iSW sub-matrix, and so forth.

$c_s^2 = 10^{-6}$ and $c_v^2 = 10^{-6}$, is modified when adding to the GC Fisher matrix progressively larger iSW sub-matrices. The first bar on the left corresponds to $\sigma_{c_s^2}$ from GC only, while the last one on the right corresponds to $\sigma_{c_s^2}$ from joint GC-iSW data. The second bar from the left corresponds to adding to GC only the $c_s^2 - c_s^2$ element of the iSW Fisher, the third to adding the $c_s^2 - \Omega_b h^2$ iSW sub-matrix, and so forth (see legend). As can be seen, if iSW were depending only on c_s^2 and were independent of all other parameters, combining iSW with GC would improve the error on c_s^2 by a factor of about 3 (see second bar from the left). Since iSW also depends on other parameters, which are correlated to c_s^2, the improvement becomes weaker and weaker the more parameters are added. Hence, when joining the data sets there is a definite improvement in measurements of these two parameters, due to the improved sensitivity to c_s^2 and c_v^2 and to the better sensitivity to all other parameters due to GC and WL. Instead, the errors on c_s^2 and c_v^2 from iSW alone become quite large after marginalizing over all other parameters, which are correlated to the sound speed and the viscosity parameter.

Also errors on c_s^2 and c_v^2 from GC are orthogonal to those from the iSW, but only in the case where $c_s^2 = 10^{-5}$ and $c_v^2 = 10^{-6}$ (see Fig. 5) this helps reducing the errors, because the former data set performs better in constraining c_v^2 and the second c_s^2. In the case of fiducial $c_s^2 = 10^{-3}$ and $c_v^2 = 10^{-4}$ it is GC which gives best errors on both parameters, while for the $c_s^2 = 1$ and $c_v^2 = 0$ fiducial model, it is weak lensing.

Another interesting question is whether iSW adds important information to that provided by the other two data sets, which had already been analysed in Sapone et al. (2013). Table 1 answers this

Table 2. Here, we indicate at how many σs it is possible to detect a nonzero sound speed or viscosity parameter.

	Fiducial $\{c_s^2,\ c_v^2\}$	Detection of $c_s^2 \neq 0$ [# of σ]	Detection of $c_v^2 \neq 0$ [# of σ]
iSW	$\{10^{-3}, 10^{-4}\}$	7.0×10^{-2}	1.6×10^{-5}
	$\{10^{-5}, 10^{-6}\}$	7.3	8.9×10^{-6}
	$\{10^{-6}, 10^{-6}\}$	2.5×10^{-3}	2.3×10^{-2}
WL	$\{10^{-3}, 10^{-4}\}$	6.4×10^{-3}	6.9×10^{-3}
	$\{10^{-5}, 10^{-6}\}$	2.7×10^{-2}	2.8×10^{-2}
	$\{10^{-6}, 10^{-6}\}$	1.4×10^{-1}	1.1
GC	$\{10^{-3}, 10^{-4}\}$	1.3×10	1.4×10
	$\{10^{-5}, 10^{-6}\}$	4.6×10^{-1}	5.2×10^{-1}
	$\{10^{-6}, 10^{-6}\}$	2.1×10^{-1}	8.1×10^{-1}
iSW+WL	$\{10^{-3}, 10^{-4}\}$	4.0	1.8×10^{-1}
	$\{10^{-5}, 10^{-6}\}$	3.8×10	1.3
	$\{10^{-6}, 10^{-6}\}$	1.4×10^{-1}	1.3
iSW+GC	$\{10^{-3}, 10^{-4}\}$	1.9×10	1.8×10
	$\{10^{-5}, 10^{-6}\}$	6.1×10	8.0×10^{-1}.
	$\{10^{-6}, 10^{-6}\}$	2.6×10^{-1}	2.4
GC+WL	$\{10^{-3}, 10^{-4}\}$	1.3×10	1.4×10
	$\{10^{-5}, 10^{-6}\}$	5.4×10^{-1}	6.0×10^{-1}
	$\{10^{-6}, 10^{-6}\}$	2.9×10^{-1}	2.1
All	$\{10^{-3}, 10^{-4}\}$	2.2×10	2.2×10
	$\{10^{-5}, 10^{-6}\}$	8.5×10	1.7
	$\{10^{-6}, 10^{-6}\}$	3.0×10^{-1}	2.9

question. It turns out that the information from iSW helps significantly in constraining c_s^2 and c_v^2 if the true model has $c_s^2 = 10^{-5}$ and $c_v^2 = 10^{-6}$, see Fig. 5. In this case, the iSW alone gives a strong constraint, which has moreover a different degeneration direction with respect to the error from galaxy clustering and weak lensing. For the other three fiducial models the gain when adding iSW is not very strong, as in both cases the combination of weak lensing and galaxy clustering gives a much tighter constraint in both the sound speed and the viscosity than the iSW alone.

It is also interesting to see at how many σs one can detect a deviation from $c_s^2 = 0$ or from $c_v^2 = 0$. This is shown in Table 2. In particular, already with iSW alone one can have a 7.3σ detection of $c_s^2 \neq 0$ for the fiducial $\{c_s^2,\ c_v^2\} = \{10^{-5},\ 10^{-6}\}$. To have a detection of more than 3σ of $c_v^2 \neq 0$ one has to combine iSW with WL or GC, where the latter observable gives a stronger detection. When combining all observables, one obtains the best detection for the fiducial $\{c_s^2,\ c_v^2\} = \{10^{-3},\ 10^{-4}\}$; for the case $\{c_s^2,\ c_v^2\} = \{10^{-5},\ 10^{-6}\}$, one has a strong detection of $c_s^2 \neq 0$ but only a 1.7σ detection of $c_v^2 \neq 0$. In the fiducial $\{c_s^2,\ c_v^2\} = \{10^{-6},\ 10^{-6}\}$ instead one detects better (at 2.9σ) $c_v^2 \neq 0$ while $c_s^2 \neq 0$ keeps being undetected.

It is interesting to notice (see Fig. 6) that when both the sound speed and the viscosity are small, but the relation between c_s^2 and c_v^2 differs from $c_s^2 \sim 10c_v^2$, the iSW effect error ellipse becomes much larger and as a result the sound speed parameter is less strongly constrained. Thus, we conclude that (*i*) very interesting results can be obtained through a combination from different cosmological probes and that (*ii*) the iSW effect is able to tighten constraints significantly for cases where there is a large difference between c_s^2 and c_v^2.

5 SUMMARY

In this paper, we have investigated how well the viscosity and sound speed of dark energy can be measured with the iSW cross-correlation spectrum, when using *Planck* and *Euclid* observations, and how joining iSW measurements to galaxy clustering and weak lensing ones improves constraints.

We found that the speed of sound is quite well constrained, with relative errors as small as 0.14 for small fiducial c_s^2 and c_v^2, while relative errors on the viscosity parameter are very large. The anisotropic stress is not well constrained by the iSW, due to the marginalization over the other parameters, which degrades the sensitivity to the sound speed and viscosity. In practice, iSW is only sensitive to c_s^2 and c_v^2 and not to the other parameters as it is for GC and WL. However, the error ellipses are interestingly orthogonal to those from weak lensing and the latter has much better sensitivity to all the other parameters. Hence, the combination of these two data sets constrains tightly the parameter space, giving relative errors on c_s^2 and c_v^2 as small as 2.6×10^{-2} and 7.5×10^{-2}, respectively. This is an improvement of a factor $\sim$1500 in the measurement of the sound speed and $\sim$50 in the measurement of the viscosity parameter, with respect to the weak lensing only constraint. The improvement obtained when combining iSW with galaxy clustering is smaller: a factor of $\sim$1.5 in c_v^2 and $\sim$150 in c_s^2. Finally, the addition of iSW to weak lensing and galaxy clustering constraints is most important if the fiducial sound speed and viscosity parameter are very small, while it is not very relevant for higher fiducial values of c_s^2.

It is also important to remind that in order to make the effect of dark energy perturbations stronger we have always used a value of the equation of state parameter $w = -0.8$. For values close to $w = -1$ the effects on the observables due to the dark energy perturbations are reduced, as all the phenomenological functions used (such as $Q(k, a)$) have a term $\propto (1 + w)$. If we use a value of $w = -0.9$ we expect our final errors on the parameters to increase. But by how much? All the observables used in this paper depend most strongly on Q^2 (see equation 15) which is intrinsically included into the matter power spectrum; for a sound speed equal to zero $Q - 1 = (1 + w)/(1 - 3w)a^{-3w}$ so the relative increase of the errors on the sound speed will be given by $1/[(Q(w = -0.9) - 1)/(Q(w = -0.8) - 1)]^2$ which is of about a factor 4 larger, in agreement also with the results found in Sapone, Kunz & Amendola (2010).

A detection of sound speed and viscosity different from the values associated with a classical scalar field, i.e. $c_s^2 = 1$ and $c_v^2 = 0$, will point to a new understanding of the accelerated phase of the Universe. This is because the non-ideal fluid considered in this paper can be thought of as en effective dark energy fluid parametrizing a modified gravity model, see Kunz & Sapone (2007). In practice, the detection of a zero sound speed does not automatically mean that we are dealing with an actual dark energy fluid, even though one would nevertheless experience effects which could be attributed to fluctuations of a fluid.

In this paper, we found that joining data from *Euclid* and *Planck* we are able to constrain simultaneously the sound speed and the viscosity parameters, provided that the two are sufficiently small. This is mostly due to the different sensitivity of the three observables, i.e. GC, WL and iSW to the two parameters. In most cases, the iSW has a different degeneracy with respect to WL and GC, and this helps reducing the errors on c_s^2 and c_v^2 by a factor of $\sim$100 (as pointed out before). Our results are in agreement with what found by Mota et al. (2007), Calabrese et al. (2011), Chang & Xu (2014), who show that for values of c_s^2 approaching $c_s^2 = 1$ the detection of a positive viscosity is very difficult, even when, as in the case of Calabrese et al. (2011), an early dark energy helps its detection by increasing its effect on smaller scales.

To conclude, are *Euclid* and *Planck* able to measure the sound speed and the viscosity parameters of a dark energy component?

If the values of c_s^2 and c_v^2 are small enough, the answer is yes; consequently, we will be able to constrain well the effective dark energy model. On the contrary, if sound speed and viscosity will escape detection, at least one of the two parameters will likely have large values. We would assume that other cosmological probes would not directly provide constraints on dark energy properties, but would nevertheless be able to provide constraining power by fixing other parts of the cosmological model, such as the dark matter density or the dark energy equation of state, which was not subject to variation in our investigation.

ACKNOWLEDGEMENTS

We acknowledge Martin Kunz and Luca Amendola for inspiring discussions. EM was supported by the Spanish MINECO's 'Centro de Excelencia Severo Ochoa'-programme under grant no. SEV-2012-0249 and by the Spanish MICINNs Juan de la Cierva programme (JCI-2010-08112), by CICYT through the project FPA-2012-31880, by the Madrid Regional Government (CAM) through the project HEPHACOS S2009/ESP-1473 under grant P-ESP-00346 and by the European Union FP7 ITN INVISIBLES (Marie Curie Actions, PITN- GA-2011- 289442). DS acknowledges financial support from the Fondecyt project number 11140496 and from the 'Anillo' project ACT1122 founded by the 'Programa de Investigación asociativa'.

REFERENCES

Amendola L., Quercellini C., Giallongo E., 2005, MNRAS, 357, 429
Amendola L., Kunz M., Sapone D., 2008, J. Cosmol. Astropart. Phys., 804, 013
Amendola L., Fogli S., Guarnizo A., Kunz M., Vollmer A., 2014, Phys. Rev. D, 89, 063538
Appleby S. A., Linder E. V., Weller J., 2013, Phys. Rev. D, 88, 043526
Archidiacono M., Lopez-Honorez L., Mena O., 2014, Phys. Rev. D, 90, 123016
Ayaita Y., Schäfer B. M., Weber M., 2012, MNRAS, 422, 3056
Baker T., Ferreira P. G., Skordis C., 2013, Phys. Rev. D, 87, 024015
Ballesteros G., 2015, J. Cosmol. Astropart. Phys., 1503, 001
Ballesteros G., Lesgourgues J., 2010, J. Cosmol. Astropart. Phys., 10, 14
Ballesteros G., Hollenstein L., Jain R. K., Kunz M., 2012, J. Cosmol. Astropart. Phys., 1205, 038
Basse T., Bjaelde O. E., Hamann J., Hannestad S., Wong Y. Y., 2014, J. Cosmol. Astropart. Phys., 1405, 021
Battye R. A., Moss A., 2006, Phys. Rev. D, 74, 041301
Battye R., Moss A., 2009, Phys. Rev. D, 80, 023531
Bean R., Doré O., 2004, Phys. Rev. D, 69, 083503
Bennett C. et al., 2013, ApJS, 208, 20
Bento M., Bertolami O., Sen A., 2002, Phys. Rev. D, 66, 043507
Bertschinger E., Zukin P., 2008, Phys. Rev. D, 78, 024015
Boubekeur L., Giusarma E., Mena O., Ramírez H., 2014, Phys. Rev. D, 90, 103512
Boughn S., Crittenden R., 2004, Nature, 427, 45
Calabrese E., de Putter R., Huterer D., Linder E. V., Melchiorri A., 2011, Phys. Rev. D, 83, 023011
Cardona W., Hollenstein L., Kunz M., 2014, J. Cosmol. Astropart. Phys., 1407, 032
Chang B., Xu L., 2014, Phys. Rev. D, 90, 027301
Chang B., Lu J., Xu L., 2014, Phys. Rev. D, 90, 103528
Crittenden R. G., Turok N., 1996, Phys. Rev. Lett., 76, 575
de Putter R., Huterer D., Linder E. V., 2010, Phys. Rev. D, 81, 103513
DeDeo S., Caldwell R. R., Steinhardt P. J., 2003, Phys. Rev. D, 67, 103509
Dossett J., Ishak M., 2013, Phys. Rev. D, 88, 103008
Douspis M., Castro P. G., Caprini C., Aghanim N., 2008, A&A, 485, 395
Erickson J. K., Caldwell R. R., Steinhardt P. J., Armendariz-Picon C., Mukhanov V., 2002, Phys. Rev. Lett., 88, 121301
Giannantonio T., Crittenden R., Nichol R., Ross A. J., 2012, MNRAS, 426, 2581
Heavens A., 2003, MNRAS, 343, 1327
Ho S., Hirata C., Padmanabhan N., Seljak U., Bahcall N., 2008, Phys. Rev. D, 78, 043519
Hu W., 1998, ApJ, 506, 485
Hu W., 1999, ApJ, 522, L21
Hu W., 2002, Phys. Rev. D, 66, 083515
Hu W., Jain B., 2004, Phys. Rev. D, 70, 043009
Jain B., Taylor A., 2003, Phys. Rev. Lett., 91, 141302
Juergens G., Schaefer B. M., 2012, MNRAS, 425, 2589
Koivisto T., Mota D. F., 2006, Phys. Rev. D, 73, 083502
Kunz M., Sapone D., 2007, Phys. Rev. Lett., 98, 121301
Laureijs R., 2009, preprint (arXiv:0912.0914)
Laureijs R. et al., 2011, preprint (arXiv:1110.3193)
Leon G., Saridakis E. N., 2011, Class. Quant. Grav., 28, 065008
Lewis A., Challinor A., Lasenby A., 2000, ApJ, 538, 473
Li W., Xu L., 2014, Eur. Phys. J., C74, 2765
Limber D. N., 1954, ApJ, 119, 655
Majerotto E. et al., 2012, MNRAS, 424, 1392
Mota D., Kristiansen J., Koivisto T., Groeneboom N., 2007, MNRAS, 382, 793
Orsi A., Baugh C., Lacey C., Cimatti A., Wang Y., Zamorani G., 2010, MNRAS, 405, 1006
Pearson J. A., 2014, Ann. Phys., 526, 318
Planck Collaboration XIII 2015, preprint (arXiv:1502.01589)
Planck Collaboration XV, 2014a, A&A, 571, A15
Planck Collaboration XVI, 2014b, A&A, 571, A16
Pogosian L., Silvestri A., Koyama K., Zhao G.-B., 2010, Phys. Rev. D, 81, 104023
Rees M., Sciama D., 1968, Nature, 217, 511
Sachs R., Wolfe A., 1967, ApJ, 147, 73
Saltas I. D., Kunz M., 2011, Phys. Rev. D, 83, 064042
Sapone D., Amendola L., 2007, preprint (arXiv:0709.2792)
Sapone D., Majerotto E., 2012, Phys. Rev. D, 85, 123529
Sapone D., Kunz M., Amendola L., 2010, Phys. Rev. D, 82, 103535
Sapone D., Majerotto E., Kunz M., Garilli B., 2013, Phys. Rev. D, 88, 043503
Sawicki I., Saltas I. D., Amendola L., Kunz M., 2013, J. Cosmol. Astropart. Phys., 1, 4
Schaefer B. M., 2009, MNRAS, 388, 1394
Schäfer B. M., Heisenberg L., 2012, MNRAS, 423, 3445
Seo H.-J., Eisenstein D. J., 2003, ApJ, 598, 720
Silvestri A., 2009, Nucl. Phys. Proc. Suppl., 194, 326
Smail I., Hogg D. W., Blandford R., Cohen J. G., Edge A. C., Djorgovski S. G., 1995, MNRAS, 277, 1
Soergel B., Giannantonio T., Weller J., Battye R. A., 2015, J. Cosmol. Astropart. Phys., 1502, 037
Song Y.-S., Hollenstein L., Caldera-Cabral G., Koyama K., 2010, J. Cosmol. Astropart. Phys., 4, 18
Takada M., 2006, Phys. Rev. D, 74, 043505
Takada M., Jain B., 2009, MNRAS, 395, 2065
Tauber J. et al., 2006, preprint (astro-ph/0604069)
Tegmark M., Taylor A., Heavens A., 1997, ApJ, 480, 22

This paper has been typeset from a TEX/LATEX file prepared by the author.